

Figure 1: A diagram illustrating our migration schema: diffusion (crimson, solid), linear (lime, dot-dashed), post-process (black, dotted), and sudden (blue, dashed), for three sets of initial and final radii and birth times. These values are pseudorandom numbers drawn from a uniform distribution for illustrative purposes. With the initial and final Galactocentric radii of a stellar population, its birth time, and one of these assumptions about the time-dependence of radial migration, the Galactocentric radius at all times is known.

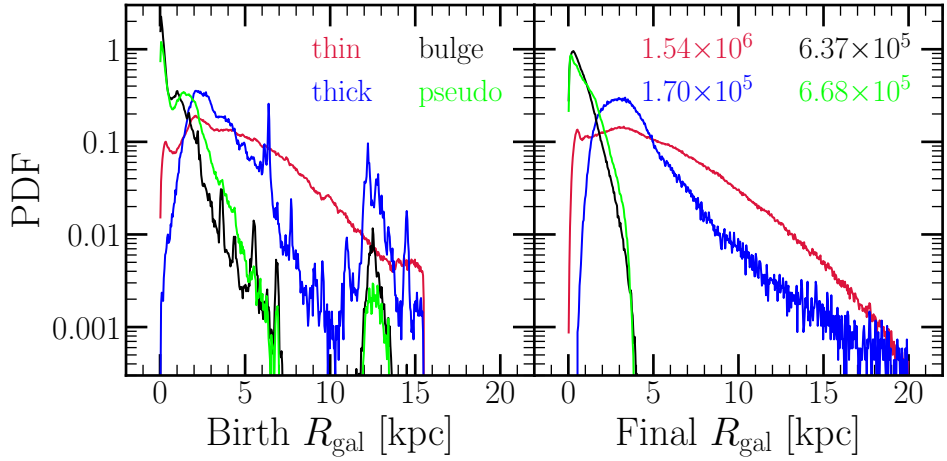


Figure 2: Distributions of h277 star particles in their birth (left) and final (right) Galactocentric radii. Distributions are shown for thin disk (crimson), thick disk (blue), bulge (black), and pseudobulge (lime) populations according to the kinematic decomposition described in § X. In the right-hand panel we denote the number of star particles in each population according to the same color-coding.

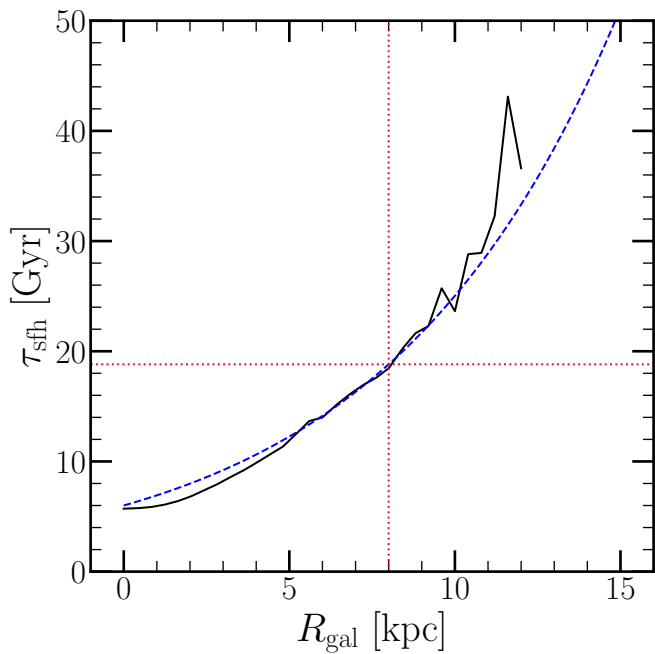


Figure 3: The e-folding timescale of the SFH as a function of Galactocentric radius adopted in this work, as reported by Sanchez (2020) for their $M_\star = 10^{10.5} M_\odot - 10^{11.0} M_\odot$ mass bin. The horizontal and vertical red dotted lines highlight $\tau_{\text{sfh}} \approx 15$ Gyr at an assumed orbital radius of the sun of $R_\odot = 8$ kpc.

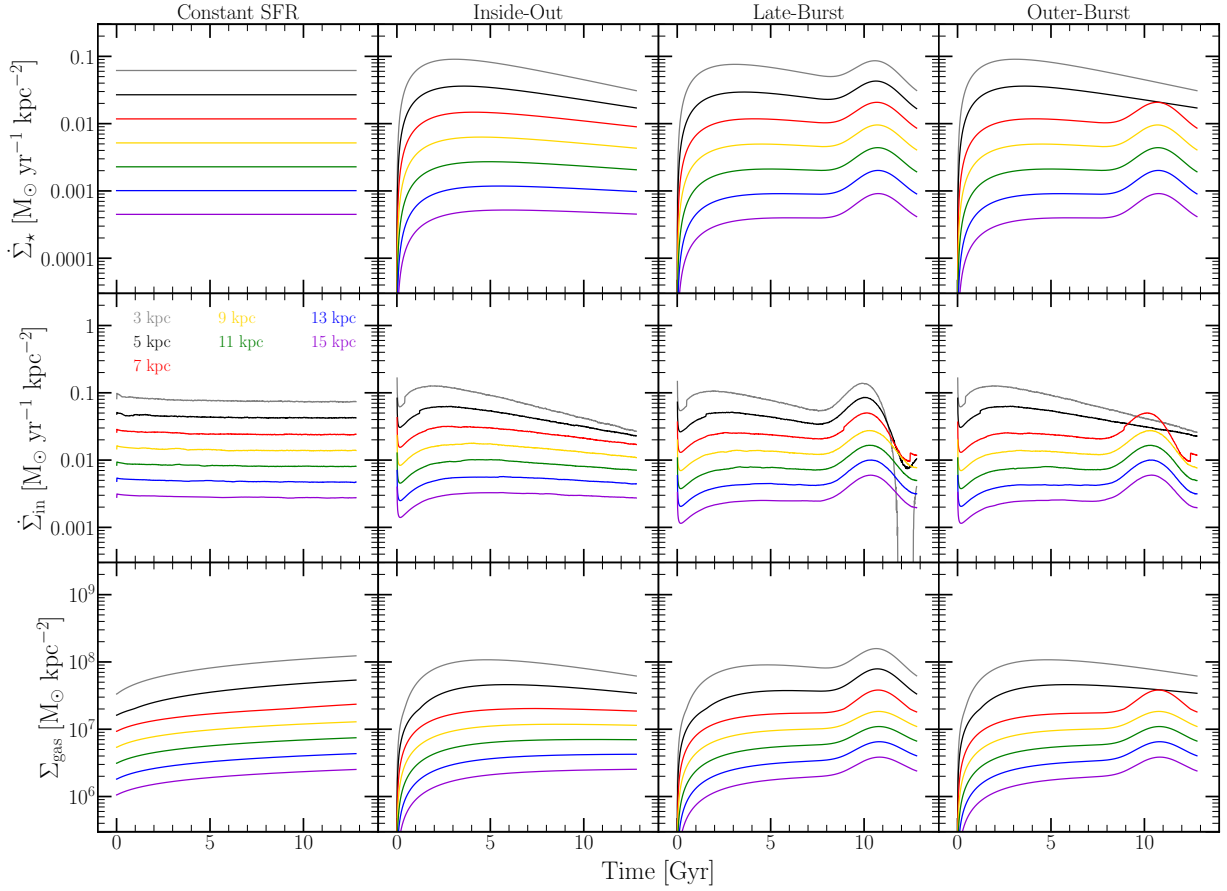


Figure 4: The surface densities of star formation $\dot{\Sigma}_*$ (top row), infall $\dot{\Sigma}_{\text{in}}$ (middle row), and gas Σ_{gas} (bottom row) as functions of simulation time in Gyr for our four fiducial models - Constant SFR (far left), inside-out (left-middle), late-burst (right-middle), and outer-burst (far right). Curves are shown for the annuli whose inner radius is 3 kpc (grey), 5 kpc (black), 7 kpc (red), 9 kpc (yellow), 11 kpc (green), 13 kpc (blue), and 15 kpc (purple).

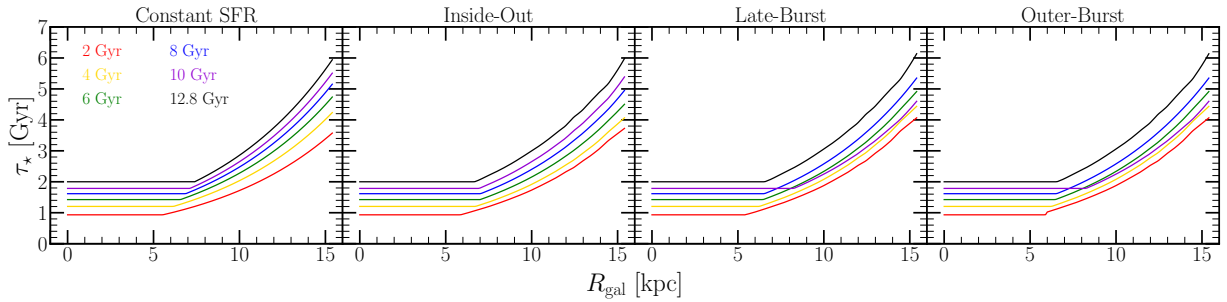


Figure 5: The star formation efficiency (SFE) timescale τ_* in Gyr as a function of Galactocentric radius at simulation times of 2 Gyr (red), 4 Gyr (yellow), 6 Gyr (green), 8 Gyr (blue), 10 Gyr (purple), and 12.8 Gyr (black) for our four fiducial models - Constant SFR (far left), inside-out (left-middle), late-burst (right-middle), and outer-burst (far right).

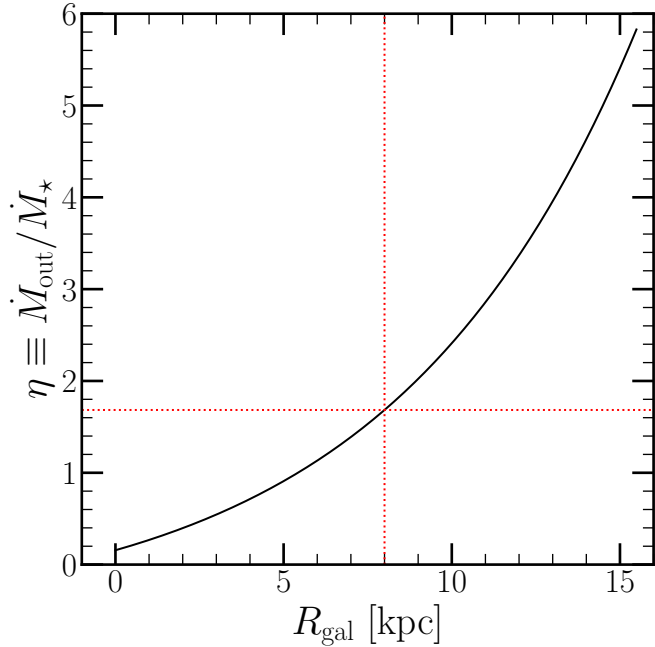


Figure 6: Our implemented scaling of the mass loading factor η with Galactocentric radius (black) as defined by equation X. The horizontal and vertical red dashed lines denote the value of $\eta \approx 1.7$ at an assumed orbital radius of the sun of $R_\odot = 8$ kpc.

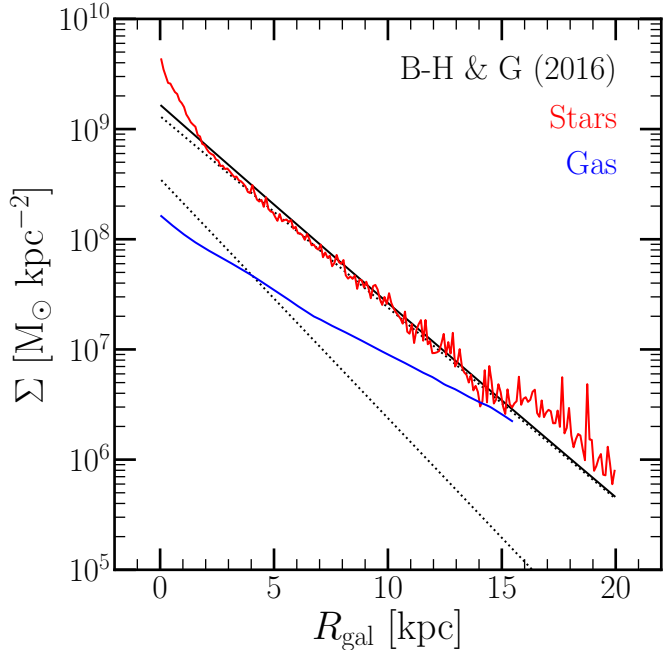


Figure 7: The surface density of gas (blue) and stars (red) as predicted by our inside-out evolutionary model with diffusion migration and $\tau_*^{\text{mol}} = (2 \text{ Gyr})(t/t_0)^{1/2}$. For comparison, we plot the surface density gradient of the Milky Way thin and thick disks as reported by Bland-Hawthorn & Gerhard (2016) in a black solid line. Black dotted lines show the individual thin and thick disk components.

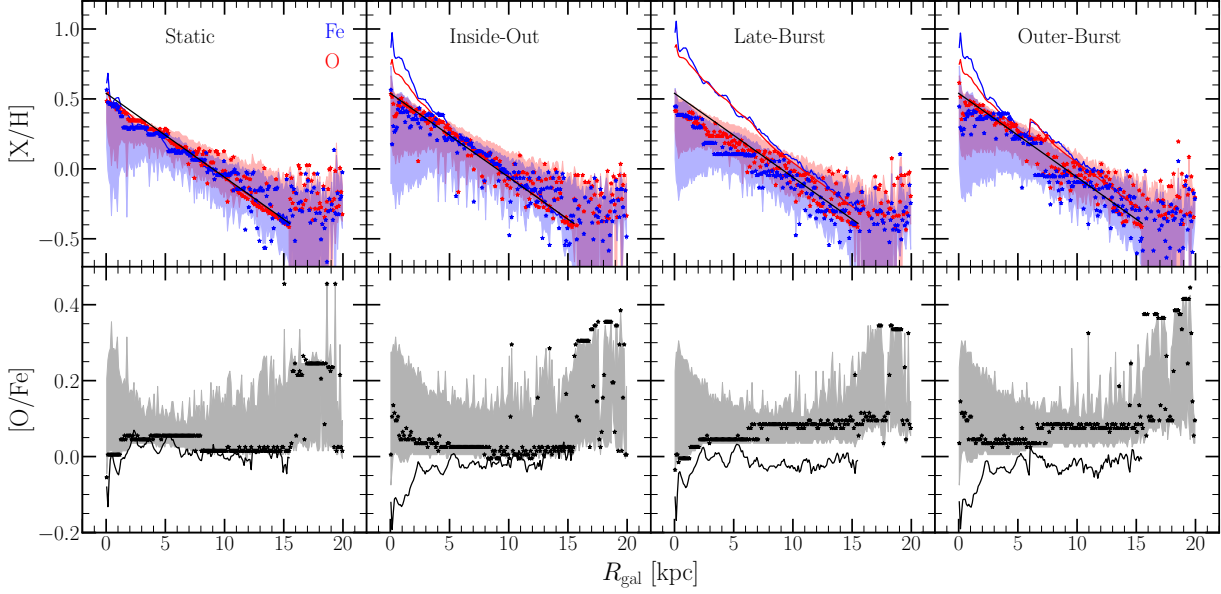


Figure 8: Radial abundance gradients in $[O/H]$ (top, red), $[Fe/H]$ (top, blue), and $[O/Fe]$ (bottom) for our four fiducial models - Constant SFR (far left), inside-out (left-middle), late-burst (right-middle), and outer-burst (far right). We plot the gas-phase abundance at the present day as a function of Galactocentric radius in solid lines. Stars denote the mode of the stellar MDF of the 100-pc width annulus at a given radius, with shaded regions marking the 16th and 84th percentiles thereof. Black lines in the top panels denote our target $[\alpha/H]$ gradient of mode($[\alpha/H]$) = +0.3 at $R_{\text{gal}} = 4$ kpc with a slope of -0.06 kpc^{-1} .

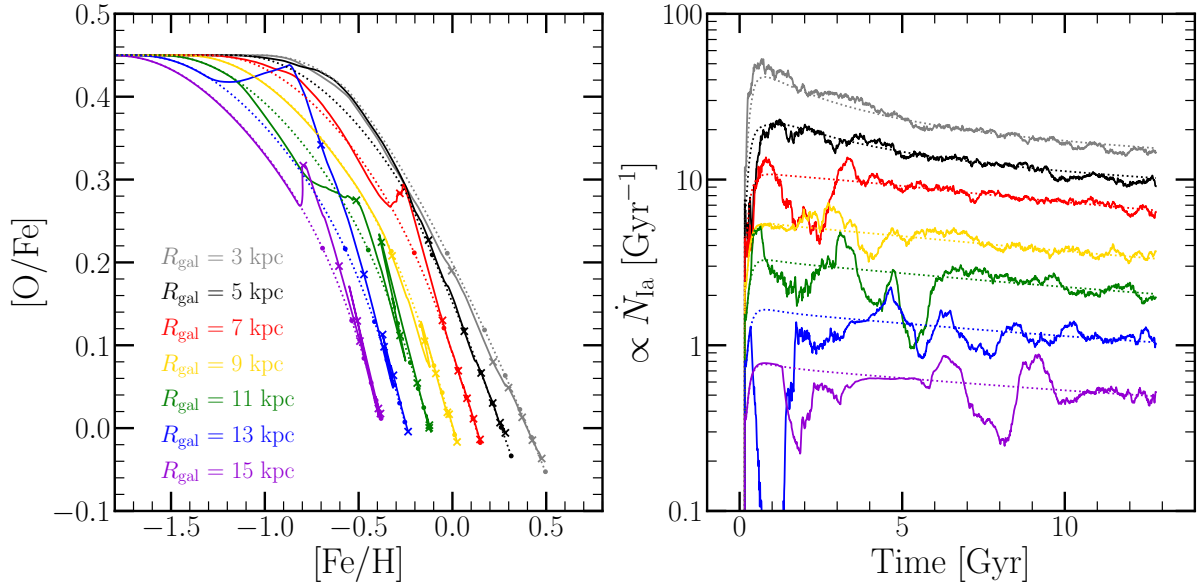


Figure 9: **Left:** Evolutionary tracks for the gas phase in the $[O/\text{Fe}]$ - $[\text{Fe}/\text{H}]$ plane for models with $\tau_*^{\text{mol}} = (2 \text{ Gyr})(t/t_0)^{1/2}$, our inside-out SFH, and either post-processing (dotted lines) or diffusion (solid lines) migration models. We plot tracks for seven annuli, color-coded according to their Galactocentric radius and denoted by the legend in the lower-left. We mark simulation times of 2, 4, 6, 8, 10, and 12.7 Gyr in X's for the diffusion model and points for the post-processing model. **Right:** The proxy for the SN Ia rate defined in equation X as a function of simulation time for the same annuli as in the left-hand panel. We multiply rates at each radii here by various prefactors in the interest of clarity.

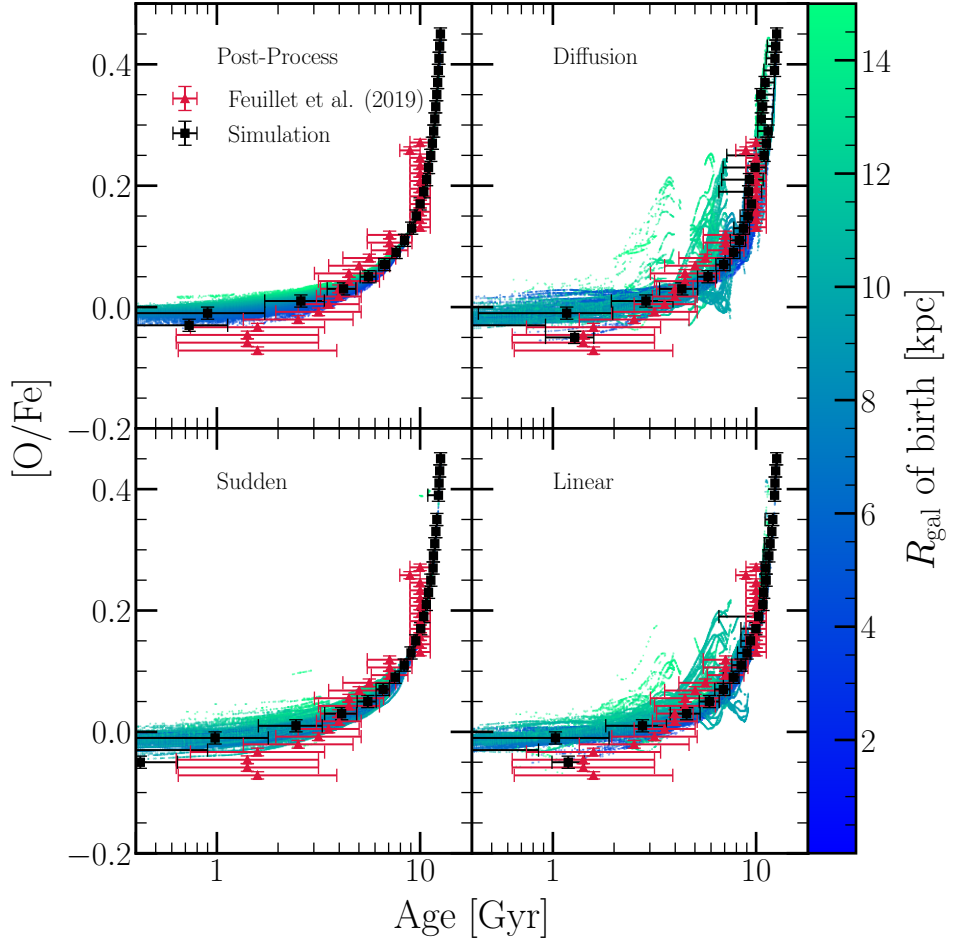


Figure 10: A comparison of the predicted age-[O/Fe] relation for the solar annulus ($R_{\text{gal}} = 7 - 9$ kpc and $|z| \leq 0.5$ kpc) between the post-processing (upper left), diffusion (upper right), sudden (lower left), and linear (lower right) migration models, assuming our inside-out SFH and $\tau_*^{\text{mol}} = (2 \text{ Gyr})(t/t_0)^{1/2}$. Red triangles and error bars denote the observed mean age and dispersion thereof in bins of [O/Fe] as reported by Feuillet et al. (2019); here we include only the bins containing at least 15 stars. Black squares denote the mass-weighted median age in 0.02-dex bins in [O/Fe], with error bars denoting the 16th and 84th percentiles of the mass-weighted age distribution in those bins. Points in the background denote each individual stellar population with a final position in the solar annulus, color-coded according to their Galactocentric radius of birth.

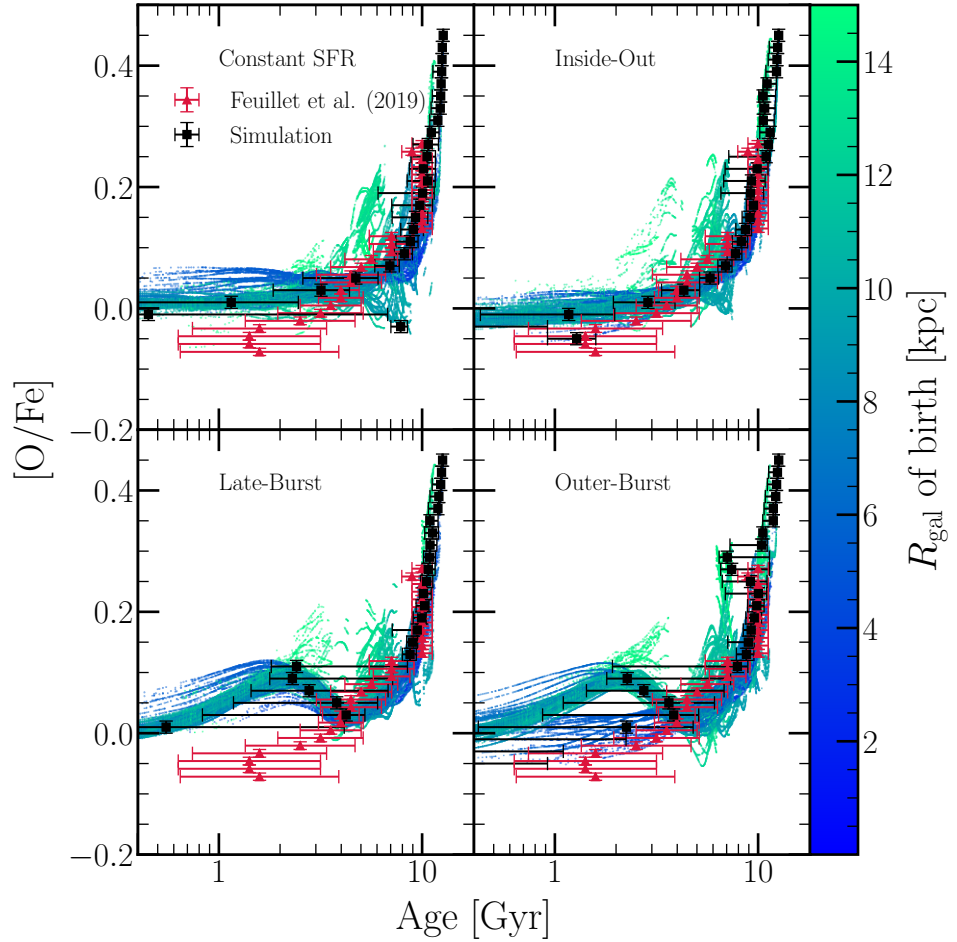


Figure 11: The same as Fig. 10, instead comparing the impact of our constant (upper left), inside-out (upper right), late-burst (lower left), and outer-burst (lower right) SFHs, assuming diffusion migration and $\tau_*^{\text{mol}} = (2 \text{ Gyr})(t/t_0)^{1/2}$.

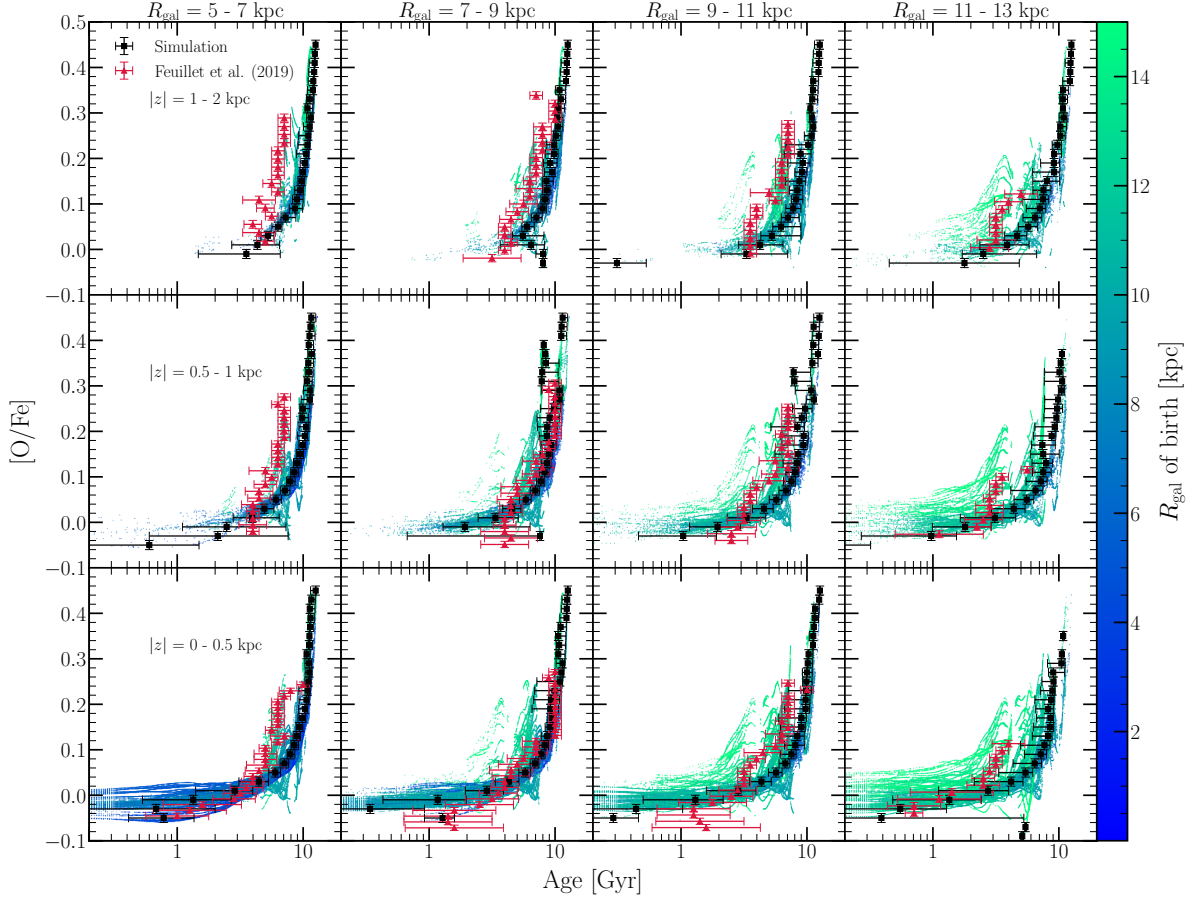


Figure 12: The age-[O/Fe] relation in different galactic regions predicted by our inside-out evolutionary model with $\tau_*^{\text{mol}} = (2 \text{ Gyr})(t/t_0)^{1/2}$ and diffusion migration. Bins in Galactocentric radius are shown in columns, and labeled at the top. Bins in the height $|z|$ above/below the disk midplane are shown in rows, noted in the left-hand column. Red triangles and error bars denote the observed mean age and dispersion thereof in bins of [O/Fe] as reported by Feuillet et al. (2019); here we include only the bins containing at least 15 stars. Black squares denote the mass-weighted median age in 0.02-dex bins in [O/Fe], with error bars denoting the 16th and 84th percentiles of the mass-weighted age distribution in those bins. Points in the background denote each individual stellar population from the simulation with a final position in that Galactic region, color-coded according to their Galactocentric radius of birth.

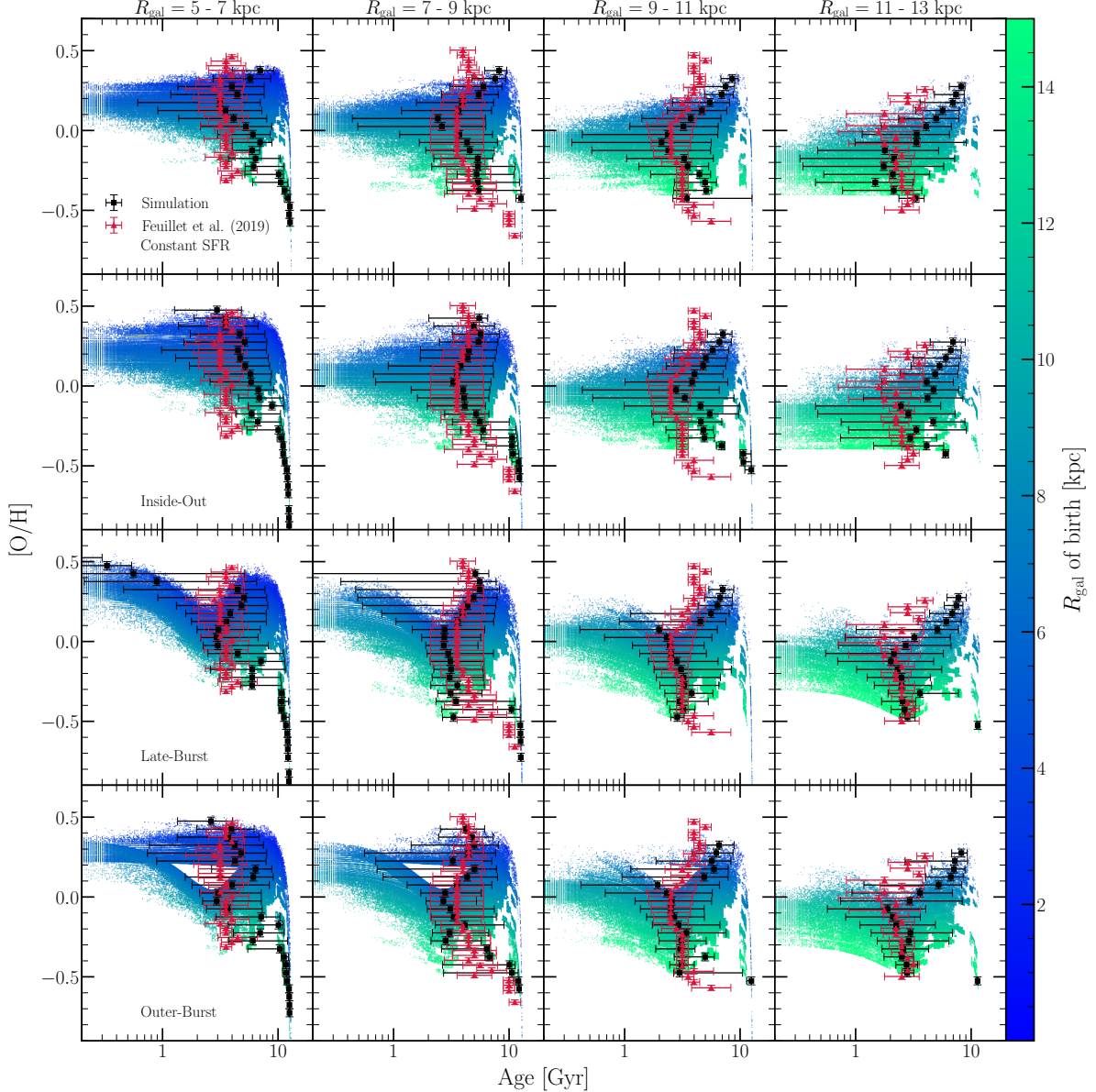


Figure 13: The age-[O/H] relation predicted by our constant (top), inside-out (top middle), late-burst (bottom middle), and outer-burst (bottom) SFHs for $R_{\text{gal}} = 5 - 7 \text{ kpc}$ (left), $7 - 9 \text{ kpc}$ (left middle), $9 - 11 \text{ kpc}$ (right middle), and $11 - 13 \text{ kpc}$ (right). Each panel plots only the $|z| \leq 0.5 \text{ kpc}$ population. Background points, red triangles with error bars, and black squares with error bars are as in Fig. 12, but with our binned, simulated relation quantified in 0.05-dex bins in [O/H].

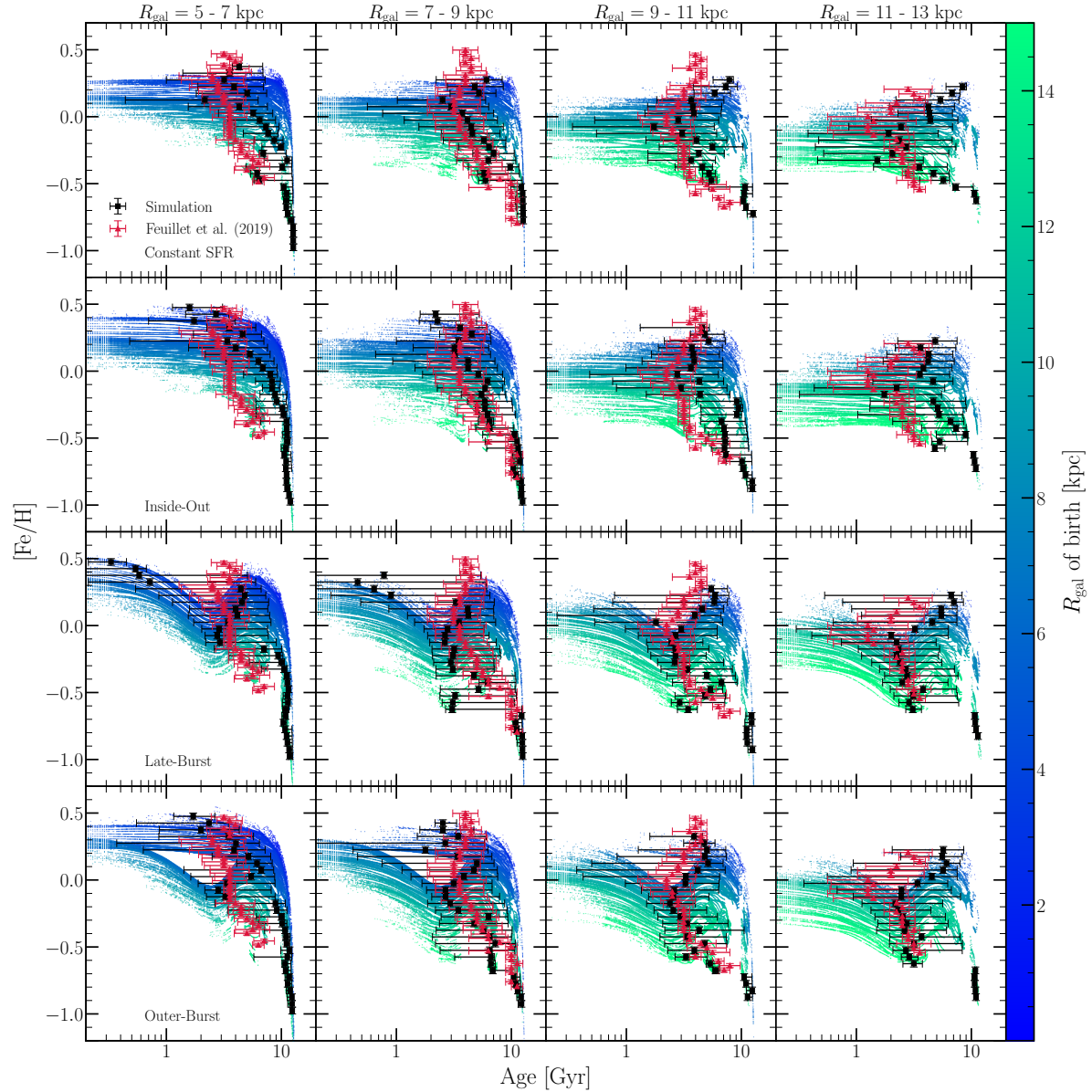


Figure 14: The same as Fig. 13, but for the age-[Fe/H] relation.

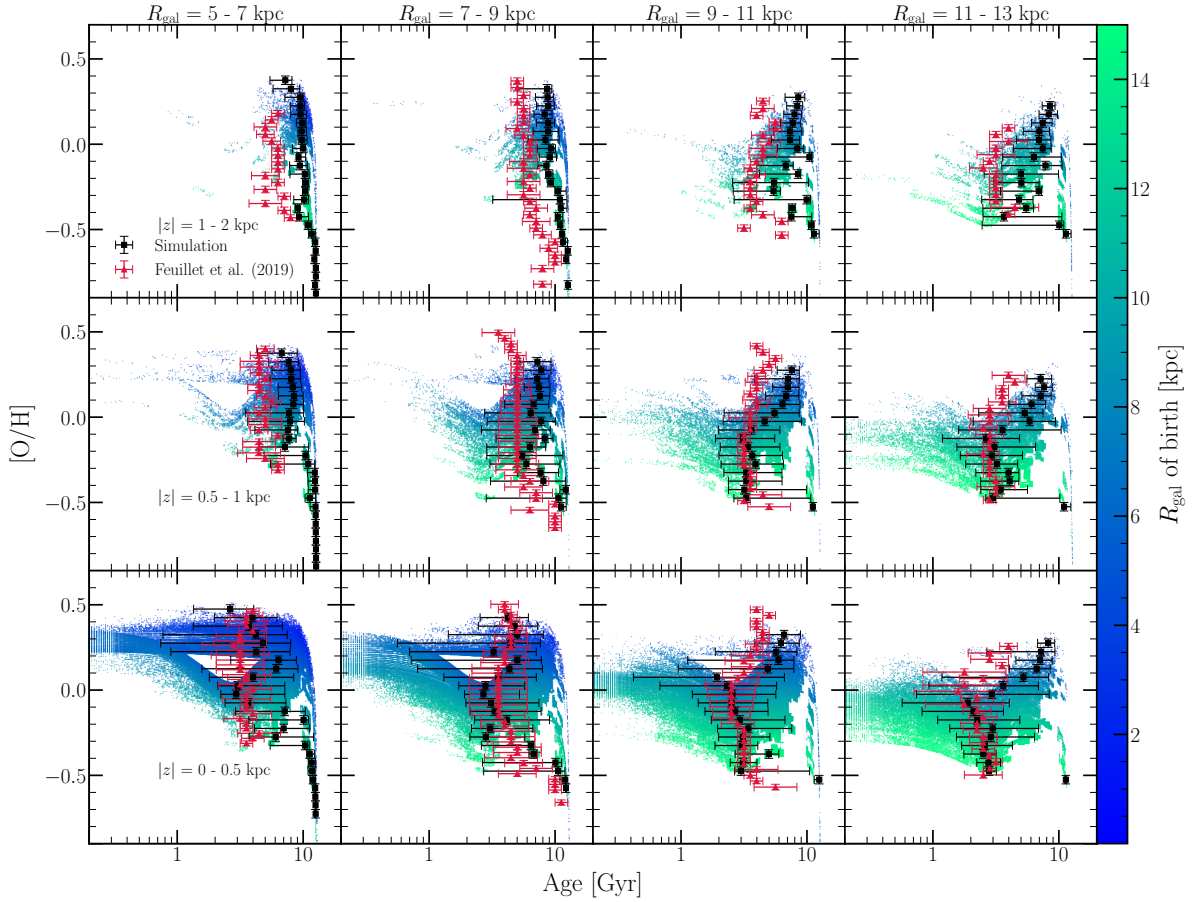


Figure 15: The same as Fig. 12, but for the age-[O/H] relation, the outer-burst rather than inside-out SFH, and with our binned, simulated relation quantified in 0.05-dex bins in [O/H].

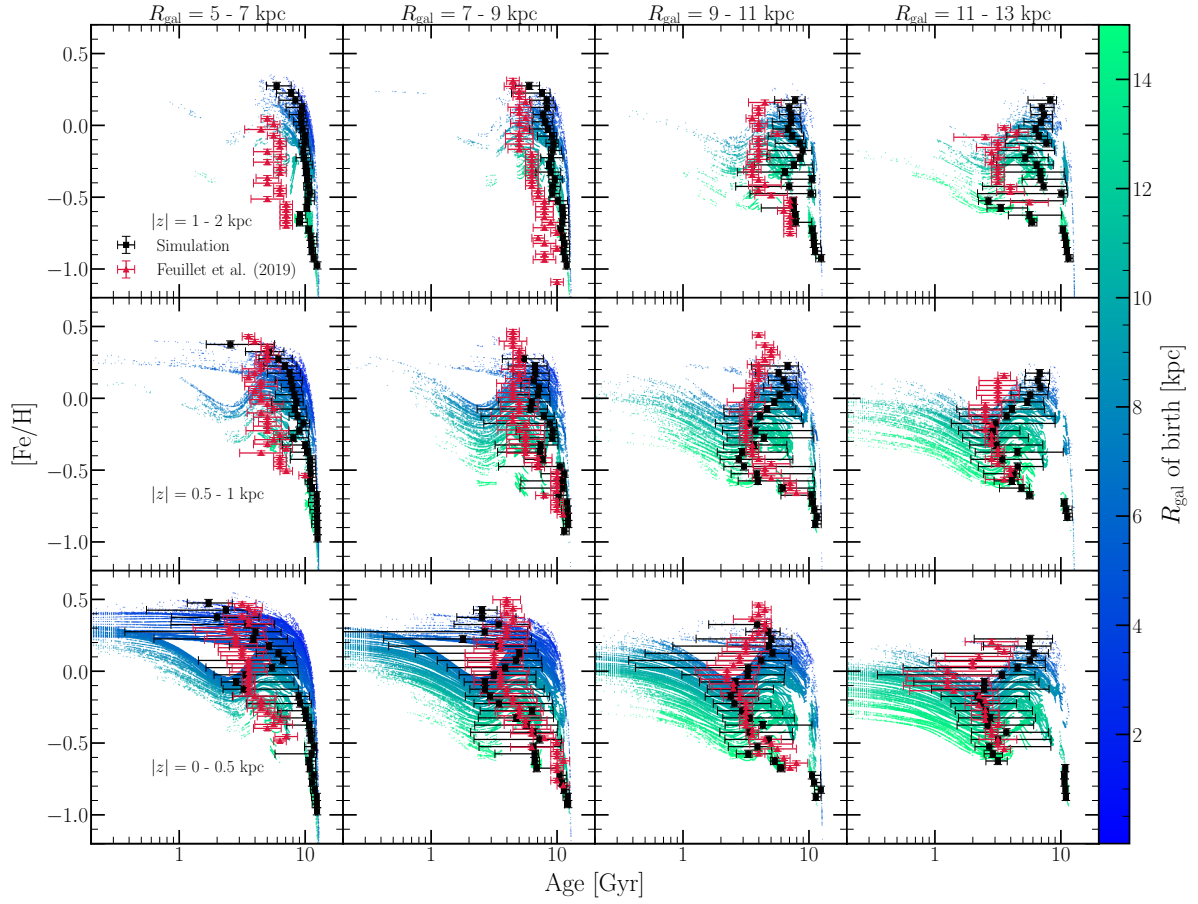


Figure 16: The same as Fig. 12, but for the age-[Fe/H] relation, the outer-burst rather than inside-out SFH, and with our binned, simulated relation quantified in 0.05-dex bin in [Fe/H].

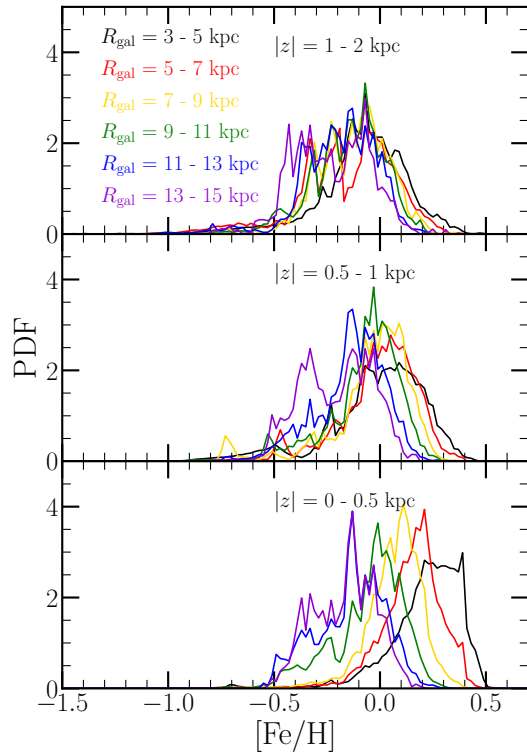


Figure 17: Metallicity distribution functions (MDFs) in $[Fe/H]$ for our inside-out SFH with $\tau_*^{\text{mol}} = (2 \text{ Gyr})(t/t_0)^{1/2}$ and diffusion migration. Distributions are shown in bins of present-day Galactocentric radius noted in the legend in the top panel, with each panel showing distributions in bins of $|z|$ noted at the top-center of each panel.

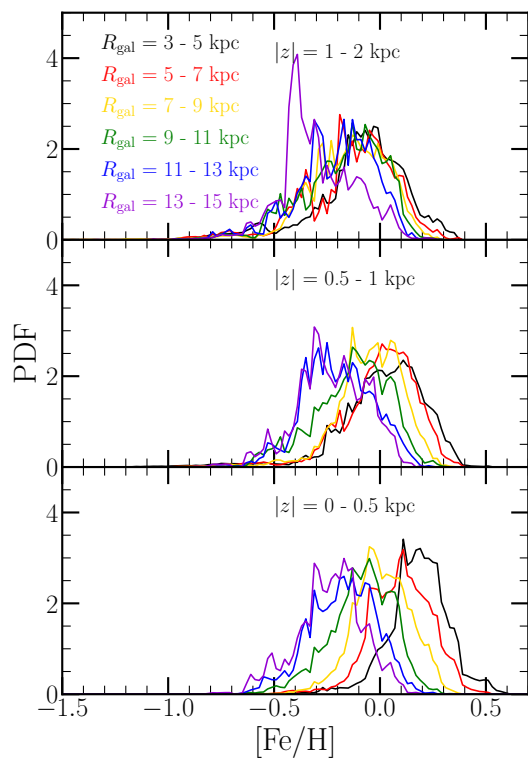


Figure 18: Same Fig. 17, but for our late-burst SFH.